Inverter-fed Drive Stator Insulation Monitoring Based on Reflection Phenomena Stimulated by Voltage Step Excitation

C. Zoeller and Th.M. Wolbank
Institute of Energy Systems and Electrical Drives,
TU Wien
Vienna, Austria

M.A. Vogelsberger
Internal Supply Chain - ISC
Bombardier Transportation Austria
Vienna, Austria

***Abstract*—Reflected wave transient phenomena in voltages and currents of inverter-fed drives caused by voltage source inverters (VSI) operating with pulse width modulation (PWM) with high dv/dt rates are well known and analyzed in many studies. The reflection phenomena occurring at the machine terminals, resulting in high overvoltages are one reason for the stress and aging mechanism of AC machines insulation system. The motivation of this work arises out of the need for a continuous monitoring of the insulation health state for traction drives systems in order to ensure high reliability of the drive over many years of operation. With a voltage step initiated by a switching transition, the inverter elicits a response in the drive system. By using the information of the resulting transient effects, conclusions can be drawn on basis of the oscillation behavior which are indicative for a change in the insulation system. Investigations in this work show that an alteration in the shape of the system transients, in peak values as well as frequency components, correlates with a dielectric insulation capability of the machine winding insulation. Measurements on a small, low voltage, random wound, induction machine (5.5kW) and a medium voltage induction machine (1.4MW) with form-wound coil based stator system are performed. Artificially induced insulation aging is realized by accelerated thermal aging to demonstrate the effect. Additionally, two different inverter types are used, with standard IGBT modules (dv/dt ~2-4kV/µs) and new SiC semiconductor inverter technology (dv/dt up to 20kV/µs), to analyze the influence of the shape of the excitation voltage step.**

Keywords— AC machines; Fault diagnosis; Insulation testing; Pulse inverters; Reflection coefficient; Traction motor drives;

I. INTRODUCTION

To keep losses in electric machines as low as possible, the currents fed into the machine terminal should be of sinusoidal shape. This would generally only be possible if the voltage supply is sinusoidal shaped and distortions by the magnetization characteristic is omitted. To generate the sinusoidal voltage with inverters, the semiconductors are used in combination with the pulse width modulation with high switching frequencies. Currently, the voltage rise times of the semiconductors in typical traction drive applications are in the range of a few hundred nanoseconds, see [1]. Due to newer upcoming wide-band gap semiconductors, e.g. silicon carbide (SiC) or gallium nitride (GaN), significantly higher dv/dt rates are possible. The incurred losses in the inverter thus be reduced and higher switching frequencies are achieved. However, the steep voltage flanks applied by the inverter generate surges within the inverter, cabling and machine winding system through reflection and oscillations. These surges strain the insulation system.

Due to this tendency the demand on insulation state monitoring systems to prevent breakdowns of modern traction drives is continuously increasing. A breakdown of a drive can be involved with high economic costs as well as significant loss of image. With the second most common faults as analyzed in [2]-[3], stator insulation faults are considered critical for a drive system, because immediate shutdown or emergency operation is necessary to prevent further damage. A combination of different stresses, e.g. high dv/dt rates as well as thermal, mechanical and environmental stress, strain the insulation system and cause a deterioration of the electrical strength [4]. In general the process usually develops very slowly over many years and also different parts of the winding would be more affected by the strains than other parts, as will be shown in a later section.

At present, methods able to estimate the health state of an insulation system like dissipation factor, tan(δ) tip-up, partial discharge PD, polarization index (PI) are based on either offline measurements or need the experience of the examiner [5]. Other methods described in [6] and [7] can be applied online with additional signal injection equipment. In [8] the surge test has been applied online for low voltage machines. The approach in this paper aims to detect imminent insulation degradation of the stator winding insulation system of the machine in a drive system without any additional signal injection source or sensor equipment. By using the inverter to generate the excitation voltage step and the integrated current sensors (closed loop-hall effect current transducers - also used for the control of the machine), the system oscillation after step excitation is analyzed and an assessment of a change in the insulation system is possible. With the opportunity of the observation of the insulation state during the operation or at least at startup or shutdown without disassembling of the drive, unexpected down times can be avoided and

The work to this investigation was supported by the Austrian Research Promotion Agency (FFG) under project number 838478.

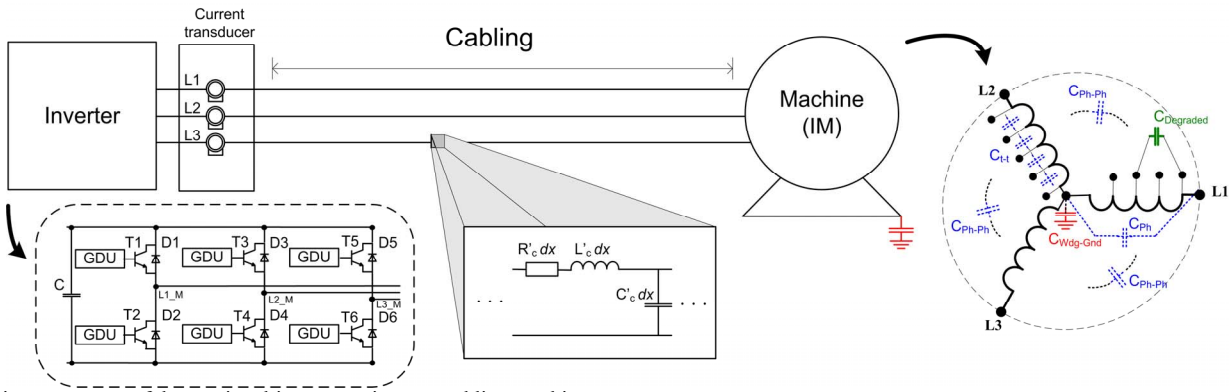

Fig. 1 Main components of the traction drive system inverter-cabling-machine.

maintenance on demand scheduled. As a consequence, system reliability can be kept high throughout expected lifetime.

II. Reflection Phenomena induced by Inverter Switching

A. Physical and Mathematical Interpretation

The approach of the proposed insulation monitoring method analyzes the high frequency characteristic of the traction drive system by the excitation with a switching transition through the connected inverter. The system can be described with its three main components: inverter, cabling, and machine, see Fig. 1. The inverter consists of three half-bridges at which every power semiconductor switch is controlled by its own gate drive unit (GDU). With the used design both switching transitions can be controlled individually by different effective gate resistors R_{G_on} and R_{G_off} within the GDU. The design with the three half-bridges is the same for the IGBT as well as for the SiC-MOSFET semiconductor inverter technology used in this work. The cabling system is represented by the distributed resistance R'_C, distributed inductance L'_C and capacitance C'_C per unit length. Finally, for the machine, besides the fundamental wave parameters R_S (stator resistance) and L_S (stator inductance), the parasitic winding parameters, i.e., winding-to-ground capacitance $C_{Wdg\text{-}Gnd}$, phase-to-phase capacitance $C_{Ph\text{-}Ph}$, phase capacitance C_{ph} and turn-to-turn capacitance $C_{t\text{-}t}$ are depicted, which largely influence the high frequency behavior and consequently the transient overvoltages at the machine terminals.

Due to the low termination impedance of the cabling (Z_C) by the inverter (Z_{In}), the reflection coefficient 'Γ' of equation (1), which is the parameter that describes, how much of an electromagnetic wave is reflected by an impedance discontinuity, is in a first approximation $Z_{In} << Z_C$. The machine winding on the other hand provides for the rapid propagated pulse a very high impedance $Z_C << Z_{Ma}$ where Z_{Ma} is the characteristic impedance of the machine. In the following explanation, the values are assumed to be ideal and the traveling wave process is assumed as lossless and on a transmission line with open end.

$$\Gamma = \frac{(Z_{Load}-Z_C)}{(Z_{Load}+Z_C)} \; where \; \begin{cases} -1 \; for \; Z_{Load} = Z_{In} \\ +1 \; for \; Z_{Load} = Z_{Ma} \end{cases} \quad (1)$$

Based on the reflection coefficients, the wave front travelling from the cabling to the machine is reflected with the same amplitude and polarity. On the other hand the returning wave to the inverter is reflected with the same amplitude but opposite sign and migrates back towards the machine. Fig. 2 depicts a scheme of a single inverter induced voltage wave, traveling on an open line with the velocity v , cf. equation (2), four times per oscillation period τ_{osc} (equation (3)) along cable length l after reaching the same voltage conditions as at start of the process, due to the reflection factors of (1). The velocity is defined by the aforementioned distributed inductance L'_C capacitance per meter C'_C uniformly distributed along the length of the line. The accurate determination of parameters L'_C and C'_C to calculate the propagation velocity is impeded, since the values vary with frequency.

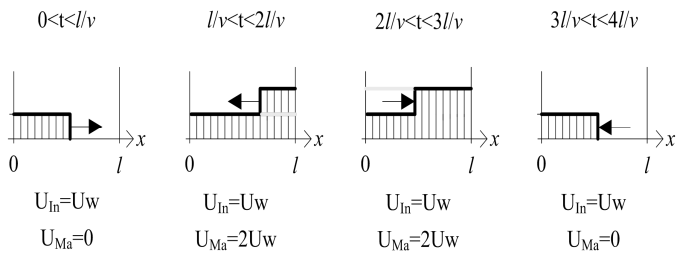

Fig. 2 Wave propagation on an open line.

$$v = \frac{1}{\sqrt{L'_C C'_C}} \quad (2) \qquad \tau_{osc} = \frac{4l}{v} \quad (3)$$

The wavelength λ is defined by the quotient of velocity of propagation v and the frequency f_0, cf. equation (4). The wavelength is estimated with decomposition of the inverter output voltage in Fourier components and with the duration of the first voltage rise $f_0 = 1/t_r$. If the length of the four time traverse of the wave is equal to the wavelength λ, after $\lambda/4$ a voltage increase at the line end and at $\lambda/2$ a voltage increase by factor 2 occurs. Thus $\lambda/2$ defines the critical cable length l_c, cf. equation (5).

$$\lambda = \frac{v}{f_0} \quad (4) \qquad l_c = \frac{\lambda}{2} = v\frac{t_r}{2} \quad (5)$$

The profile of an inverter output voltage surge is simplified adopted to

$$g(t) = \begin{cases} 0 \; for \; t < 0 \\ 1 \; for \; t > 0 \end{cases} \quad (6)$$

The incident wave from the inverter output in the time slot 0<t<*l*/*v* is defined by

$$u(x,t) = \hat{u}g(t - x/v) \quad (7)$$

With the reflection coefficients in (1) the voltage distribution is given by

$$u(x,t) = \hat{u}\left[g\left(t - \frac{x}{v}\right) + g\left(t + \frac{x}{v} - \frac{2l}{v}\right) - g\left(t - \frac{x}{v} - \frac{2l}{v}\right) - g\left(t - \frac{x}{v} - \frac{4l}{v}\right) + \cdots\right] \quad (8)$$

These assumptions represent only a simple model of the reflection process. A decomposition of the pulse shaped wave in a continuous spectrum of sine waves show that individual components propagate at different speeds caused by reflections and material dispersion. The wave shows typically dispersive character.

In practical systems the reflection can result in an overvoltage reaching up to 2 p.u. of the inverter output voltage according to [9] and up to 4 p.u. according to [10], even if only in theoretical considerations. On the machine side the increased voltage level additionally strains the insulation. In addition to the reflection coefficient the peak value of the overvoltage mainly depends on the voltage rise time t_r of the voltage pulse applied by the inverter and the cable length l_C between inverter and machine. The level of overvoltage also depends on the initial condition of trapped charge due to multiple PWM pulses and the interaction between cable transient damping characteristics and machine dynamic surge impedance.

A multiplicative factor for the increase in voltage at the machine terminals is assumed, as stated in [11]. With equation (9) the approximated overvoltage at the machine side in percentage k_{ov} is calculated considering the aforementioned factors and the propagation speed v.

$$k_{ov} = \frac{\frac{1}{t_r}(3 * l_C * \Gamma)}{v} = \frac{1}{t_r}\frac{3 * l_C * \Gamma}{\frac{1}{\sqrt{C'_C * L'_C}}}$$
$$where \; \Gamma = \frac{Z_{Ma} - Z_C}{Z_{Ma} + Z_C} = \frac{(Z_{Ma} - \sqrt{\frac{L_C}{C_C}}))}{\left(\sqrt{\frac{L_C}{C_C}} - Z_{Ma}\right)} \quad (9)$$

With the availability of winding taps, the analysis of the voltage distribution within the machine is possible. This shows that overvoltage not only occurs at the windings terminal end, but also on subsequent coils within the machine and the maximum factor of the overvoltage does not mandatorily occur at the first coil of the machine.

B. Voltage Reflection and Inverter SwitchingTransition

Generally, inverter and machine are connected by basic three wire system plus ground connection. The windings of all machines in this work are in star circuit configuration. The PWM modulated inverter typically switches only one half-bridge at a time. There are always two parallel inverter legs in steady state. Thus, at most switching patterns, two inverter outputs are both connected to positive or negative dc link voltage, while the remaining output is connected to opposite polarity, as depicted with a scheme of the machine winding in Fig. 3 (a). The figure shows a positive excitation in phase L1 and is denoted with differential mode, since there is one line for the incident wave travelling to the machine, partially reflected and partially transmitted into the machine winding, and two parallel connected lines as the return line of the current. Fig. 3 (b) depicts the situation where all inverter outputs are connected to the same potential, either positive or negative DC-link voltage, denoted with common mode [12]. In this case no current is directly flowing into the machine, since all machine phases have the same voltage potential. However, common mode currents occur due to the inverter-induced hf common mode voltage [13]. The common mode current characteristic is mainly described by the parasitic winding capacitances of the machine, which are mostly negligible considering fundamental wave operation only.

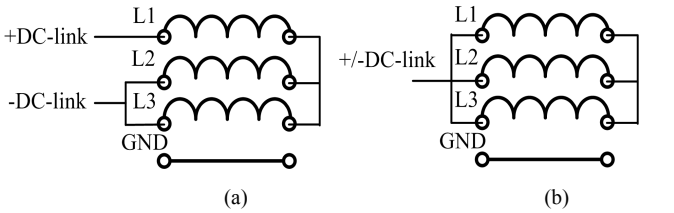

Fig. 3 Machine winding (a) differential mode switching (b) common mode switching of inverter.

Due to these scenarios the parasitic machine winding parameters are further analyzed. With frequency response analysis and LCR meter measurements the parameters are investigated in differential as well as common mode operation and are presented in a later section IV for further interpretation.

Investigations in this paper are done on a small low voltage random wound induction machine (5.5kW) as well as a medium voltage induction machine (1.4MW) with form-wound coils based winding system. The cable length between the inverter and the machine is 12m. To apply a voltage step to the system that elicits the high frequency behavior, different ways to establish the corresponding inverter output voltage step are possible. For the following explanations and illustrations the excitation is described for a measurement of phase L1 with a switching transition starting with all three phases connected to low side of the dc link potential (lower short-circuit) and then initiate a transition of the corresponding inverter leg by turning off the low side transistor and turning on the high side one of the corresponding phase L1, as this switching transition also occur during operation of the drive. The machine is not magnetized and the rotor stands still. Fig. 4

(a) and (b) depict the voltage of the inverter output '*L1*' (blue trace) and the voltage of phase terminal L1 at machine side with respect to lower DC-link potential (green trace) as well as the current measured in phase L1 (red trace) close to the inverter side, cf. position current transducers in Fig. 1. In subfigure (a) the IGBT inverter is used as a source of excitation with a significantly lower dv/dt (~2kV/µs) voltage rise rate than used at the measurements presented in subfigure (b) with the SiC-MOSFET inverter (up to 20kV/µs).

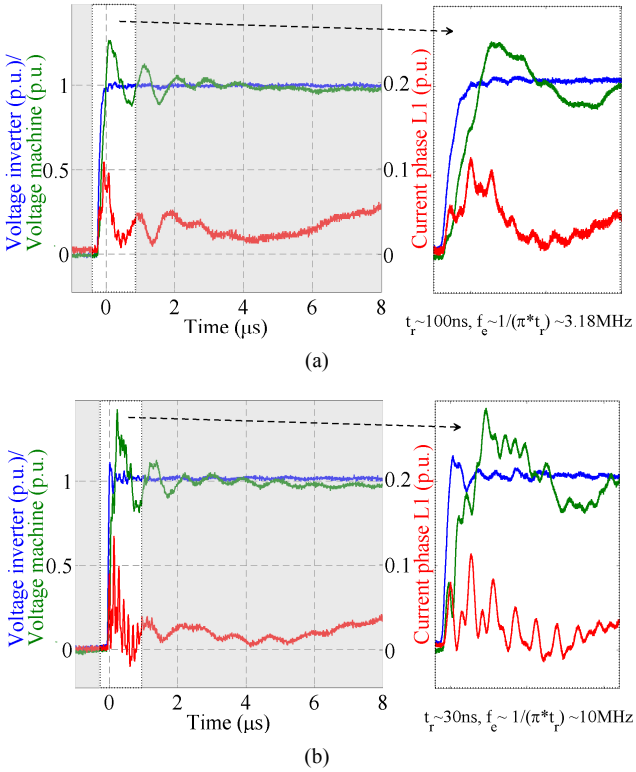

Fig. 4 Voltage to lower DC-link potential of the inverter output 'L1' (blue) and machine-terminal L1 (green) with current trace L1 at the inverter side (red) for two different inverter systems (a) IGBT-inverter and (b) SiC inverter.

The overvoltage and the high frequency resonances occurring after a switching transition of the inverter are clearly observable in both cases. The overvoltage shows a damped behavior with decaying oscillation. The fundamental period of this oscillation is independent of the voltage rise time and resonance occurs in the machine winding. The overvoltage measured at phase terminal L1 is about 30% in case of subfigure (a) and about 45% in subfigure (b) with the SiC-MOSFET inverter and higher dv/dt voltage rise rate. These results indicate a match of the relationship of increasing overvoltage values with lower rise time. The results also show that the critical cable length is not reached and the overvoltage is < 2 p.u.. Individual partial reflections are visible on the side of the machine during the voltage rising at the inverter. Fourier analysis of the voltage step defines an equivalent high frequency that corresponds to the step rise time, as depicted under the zoomed area of both cases. During the reflection on the machine side, not only the amplitude is increased in accordance with the corresponding reflection coefficient, it also increases the rate of voltage rise. The increase in the rate of voltage rise is not significant for the effects on the cabling, because the shape of the wavefront does not change. However, the voltage distribution inside the machine winding is affected due to the higher steepness which causes inhomogeneous voltage distribution across the windings. The voltage overshoot shown above in Fig. 4 affects as an increased stress the main insulation. By contrast the non-linear voltage distribution acts on the inter-turn insulation and can result in arcing between adjacent turns of the coil or other arcing over several turns.

Alternative excitation methods analyzed for this work are for instance, upper short-circuit of all phases and initiating the transition by turning off the high side transistors and turning on the low side transistors of the two remaining phases L2, L3 for an indirect excitation of phase L1. In addition, here are shown in Fig. 5 that a change in the excitation method with a switching transition from high DC-link level to low DC-link level applied to phases L2 and L3, while retaining L1 on high DC-link level, has a significant influence on the course of the current. In this case the reflection phenomenon has additionally changed, with a slightly lower overvoltage. This is also visible in the transient part of the (lower) current trace. The capacitive coupling of the current sensor with this type of excitation has also changed due to the constant voltage level of the primary conductor through the current transducer.

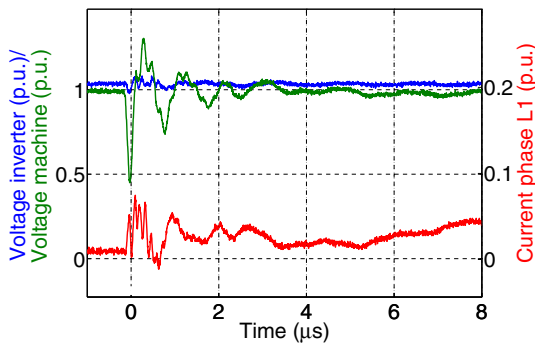

Fig. 5 Voltage to lower DC-link potential of the inverter output 'L1' (blue) and machine-terminal L1 (green) with current phase L1 at indirect excitation of phase L1 (IGBT-inverter).

At the last mentioned excitation method some interesting aspects have to be considered regarding the commutation from semiconductor switch to the parallel diode, especially during non-zero phase current. Investigations showed that the shape of the voltage step is influenced whether the IGBT or the diode is conducting and thus the reflection phenomenon is also changed accordingly. This can be explained by changing output impedance in the various cases.

C. Current Transient Signal Properties

In addition to the reflection phenomena of the voltage, the current traces also show a transient decaying behavior after the switching transition. As will be shown in sections III and IV the parameters which are mainly influencing this oscillation process are the parasitic insulation capacitances. These parasitic capacitances are influenced by the insulation health state. This in turn means that a change in the insulation state,

influences the relation between the impedance of the cable and machine Z_C respectively Z_{Ma}. As a result, the occurring frequency components in the transient part of the current signal will also change during the aging process. This is illustrated with Fig. 6 that depicts the transient current responses of the machine in case of the healthy machine state (denoted with '*Healthy*') and the same machine with changed impedance of the winding by adding a capacitor of 7.5nF parallel to the first coil of phase L1, denoted with '*Degraded Insulation*'.

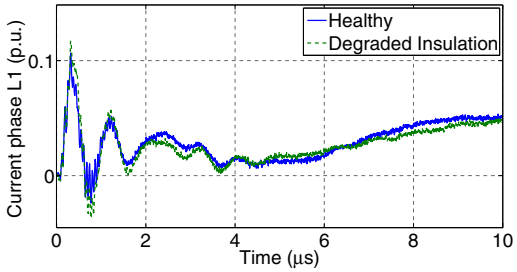

Fig. 6 Effect of insulation degradation (emulated with capacitor parallel to 1st coil phase L1) on transient current response.

Another influence on the current transient that has to be considered depicts Fig. 7. The voltage and current measurement are conducted after voltage step excitation by the IGBT inverter as shown in Fig. 4 (a), with the difference that the position of the current measurement was placed near to the machine side. A significant change in the current trace is visible with a delayed start of the oscillation and partly other frequency components. Thus, it is important for the following investigations that current measurement is done at exactly the same position for a comparison.

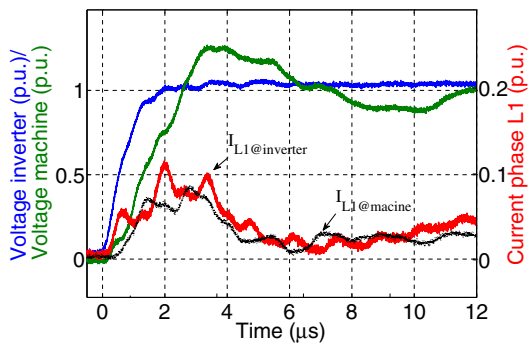

Fig. 7 Voltage to lower DC-link potential of the inverter output 'L1' (blue) and machine-terminal L1 (green) with current trace L1 at the inverter side (red) and measured at machine terminal (black).

III. Aging Effects at Stator Winding System

The insulation degradation process is a slowly developing process that finally speeds up in an insulation breakdown, usually starting first with the turn-to-turn insulation and leading to higher severity faults like phase-to-phase or phase-to-ground respectively that lead to a breakdown of the whole drive. By accelerated aging of the insulation with cycles of thermal exposure, the effects of fatigue behavior of different stator winding insulation systems are investigated. At the beginning of each aging cycle different diagnostic methods are used for insulation state evaluation and the measurements are conducted at each cycle in the same order. First, LCR-meter and non-destructive and sensitive frequency response analyzer 'FRA' measurements are carried out. After that, the capacitance and dissipation factor measurements at nominal voltage are determined, followed by transient current signal evaluation after inverter step excitation. Finally, a voltage withstand test was applied to test the insulation strength and to define a failure criterion. The measurements are conducted at defined ambient temperature (25°C) as well as controlled humidity. The results show that the main parameter that is linked with insulation degradation is the insulation capacitance.

In Fig. 8 (a) the stator winding system of the low power machine (5.5kW) in the healthy state (upper subfigure) and after 9 thermal aging cycles, (class F, aging temperature ϑ_{aging}=220°C and exposure period 2 days/cycle) is depicted. Temperature and exposure period were chosen in accordance with the IEEE standard 1707 with the target to reach up to ten cycles until failure of the insulation system is validated by a voltage withstand test. The capacitance measurement shows a decrease of the capacitance between 10kHz and 100kHz of about 25%.

In subfigure (b) the stator insulation system of a 1.4MW induction machine is tested by analyzing the behavior of a specimen consisting of six form wound coils inserted in a stator slot model (motorette).

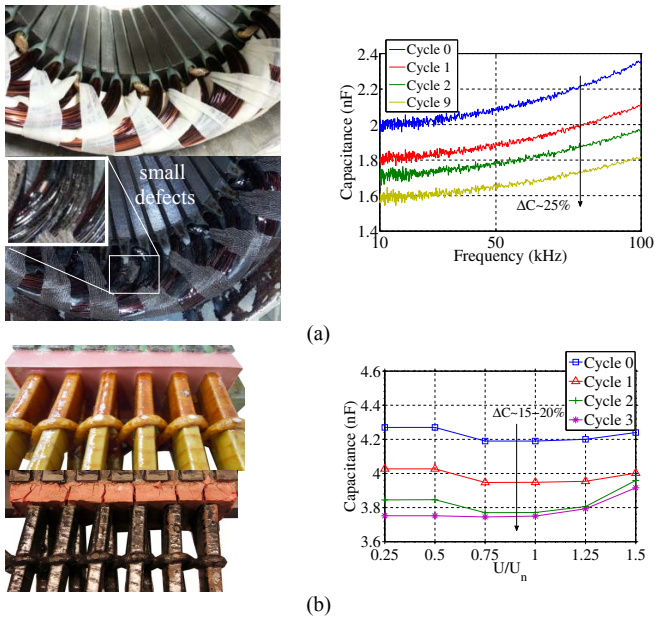

Fig. 8 (a) 5.5kW induction machine and (b) stator slot specimen (motorette) of the medium voltage insulation system applied to accelerated aging cycles.

The insulation system is the same as in the machine, based on a combination of mica tapes, polyimide film/glass-fibre, woven glass tapes for the conductor insulation and impregnating resins for the groundwall insulation. The results show that the capacitance values tested at different levels of the nominal voltage have changed with increasing number of applied aging cycles (aging cycles according to IEEE-1776). Thus, the effect of a change of insulation capacitance during

aging of an insulation system can be observed at low voltage tests over a wide frequency range Fig. 8 (a) as well as at high voltage tests subfigure (b).

IV. Current Transients and Insulation Health State Estimation

A. Results of Random Wound Induction Machine

Target of the approach is to detect incipient stator insulation defects based on the transient current response recorded with the same current transducers of the drive system already used for machine control (typical bandwidth specification: DC to $f_{H(-3dB)}$ ~150-300 kHz; maximum di/dt 50A/µs). The machine is excited using the IGBT inverter. The changes of the winding capacitance analyzed are either artificially evoked by placing capacitors parallel to the winding using tabs, or caused by aging with thermal aging cycles. In Fig. 9 (a) the transient current response of phase L3 (5.5kW machine) for the healthy machine state (blue trace) and in case of artificially emulated insulation degradation (470pF capacitor parallel to phase L3 – dashed green) are shown. In Fig. 9 (b), as comparison, the transient current response of the same machine is depicted again for the healthy machine (blue trace) and with actually degraded insulation after eight aging cycles (dashed red). In both sub figures the transient characteristic has significantly changed. Regarding the LCR meter and FRA parameter estimation, the change of the capacitance value caused by nine aging cycles is in a range of ΔC~400pF, cf. Fig. 8 (a). Despite the capacitance deviation being of the same magnitude in both scenarios, in case of the parallel capacitor the major change is in the high frequency part of the current signal, whereas aging leads to a change in the lower frequency range. In case of the emulated insulation degradation with the parallel capacitor, the capacitance of the system is increased and due to the aging cycles the capacitance is reduced. However, key factor of the method is the detection of insulation degradation by any change of the current transient. Complementary the results of phase L1 and L2 are depicted in subfigures (c) and (d). Both show similar changes compared to phase L3. During *'Cycle 8'*, the voltage withstand test (1000V dc) of phase L3 against ground failed for the first time. According to the standard test procedure, this machine has not passed the test. However, inverter operation (test pulses with dc-link voltage 440V) was still possible and so the cycles were continued. Thus *'Cycle 8'* and *'Cycle 9'* represent the machine insulation at a final stage. It should be mentioned that although phases L1 and L2 passed the voltage withstand test, the deviation of the transient current response by excitation with the inverter in the corresponding phases, is still visible through the effect of the resonance within the machine and the Y-connected winding configuration. Thus, indirect monitoring of insulation state of other phases is possible and redundancy of the system exists even in a two current sensors configuration or when a failure of single sensor occurs in three sensor configuration, however, then accuracy of detection is reduced.

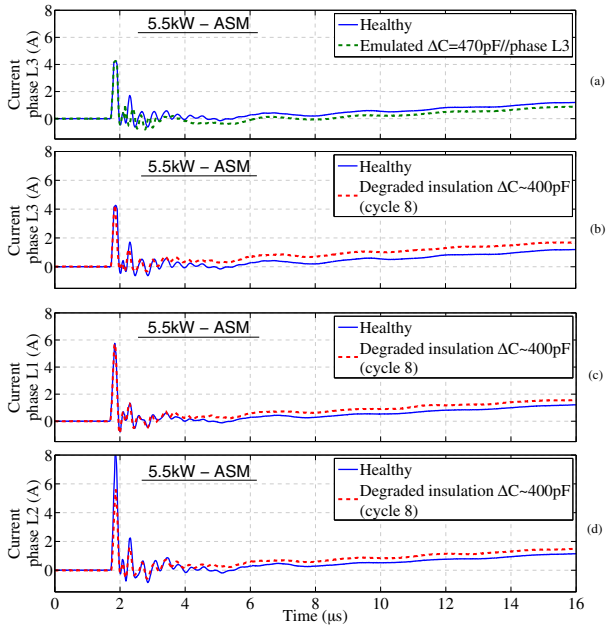

Fig. 9 Transient current response after inverter voltage step excitation of 5.5kW machine for 'Healthy' machine state compared to (a) emulated insulation degradation with capacitor parallel to phase L3 (b) after 8 aging cycles phase L3 (c) after 8 aging cycles phase L1 and (d) after 8 aging cycles phase L2.

For further interpretation the current transients are analyzed in the frequency range, as depicted in Fig. 10 with the amplitude spectrum of the transient current response for different winding insulation health states of phase L3. A decrease of frequency components especially in the lower range from 50kHz to 350kHz is observable and is in accordance with decrease in the global capacitance, resulting a change of all parasitic capacitances (turn-to-turn, phase-to-phase etc.). It is also evident that the winding state with the artificially added capacitor tends in the opposite direction with increased frequency components (dashed gray).

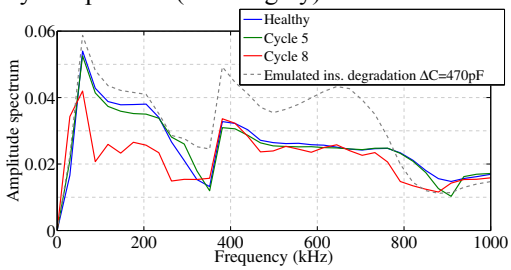

Fig. 10 Spectra of transient current time signals of Fig. 9 (a) and (b).

Based on the change of the amplitude spectrum in a range up to 1MHz an insulation state indicator (ISI) is calculated with the root mean square deviation (rmsd) for every equidistant frequency point between the trace of '*Healthy*' and the further winding insulation scenarios. Further details of the indicator calculation are given in [14]. The calculated indicator values for phase L3 are depicted in Fig. 11. To further increase accuracy, the measurements are repeated 50 times and the mean values are taken for further analysis. The machine state denoted with '*Cycle 0'* corresponds to the healthy machine

state. All further measurements are related to this healthy value and thus a value greater than 1 indicates a change of the insulation state. From value '*Cycle 0*' to value '*Cycle 1*' there is a clear increase in the indicator. This increase continues until '*Cycle 5*', '*Cycle 8*' and '*Cycle 9*'. However, according to the defined offline test procedure (withstand voltage according IEEE standard) the machine winding has not passed '*Cycle 8*' and '*Cycle 9*' and further maintenance steps are necessary, because imminent total failure is probably. The box-plot in Fig. 11 represents variance of several measurements taken after each cycle.

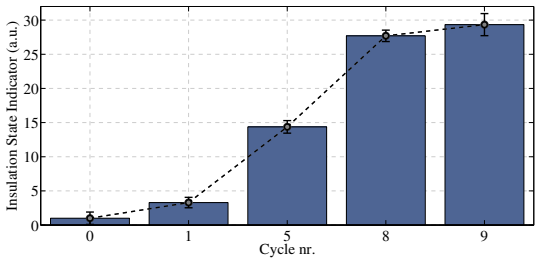

Fig. 11 Insulation State Indicator calculated by rmsd of spectra phase L3 after applied aging cycles.

The capacitance change per phase from healthy machine state to the final value before outage of the machine is about 400pF for the phase-to-ground capacitance. The total phase-to-ground capacitance for the healthy machine was estimated with common mode operation (cf. Fig. 3 b) and RLC measurement to 2.029nF which results in a deviation of about 25%. The measurement of phase-to-phase capacitance is estimated with arrangement depicted in Fig. 12, with L2 and L3 short circuited and connected to ground. The total capacity C_{total} is the sum of the capacitance against the frame and the capacitive coupling to the other strands, which are assumed to be equal and was measured to 4.829nF.

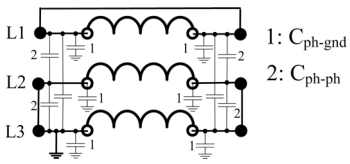

Fig. 12 Measurement of capacitance C_{total} against frame

With the following relation (10) and (11) the phase-to-phase capacitance C_{ph-ph} is calculated.

$$C_{total} = C_{ph-gnd} + 2C_{ph-ph} = 4.829nF \quad (10)$$

$$C_{ph-ph} = \frac{1}{2}\left(C_{total} - C_{ph-gnd}\right) = 1.4nF \quad (11)$$

The change due to aging of the phase-to-phase capacitance is 230pF which is about 16% change from the initial value. The value of the indicator of the proposed method has increased with a factor around 20.

B. Medium Voltage Induction Machine

In Fig. 13 the upper and lower subfigure shows the current transient of the motorette and of phase L3 (1.4MW machine) after the system is excited by SiC-MOSFET inverter. Again insulation degradation emulated with a capacitor in parallel to parts of the specimen and degradation caused by thermal aging cycles is compared. Similar observations as in the previous tests are visible. According to Fig. 13 the measured capacitance change of the motorette against ground is 400pF, cf. Fig. 8 (b). The change is visible comparing the healthy motorette state (blue trace) and the trace after accelerated aging (green trace). The change of the transient by placing a capacitor parallel to the coils, comparable to the capacitance variation due to aging is depicted with the red trace.

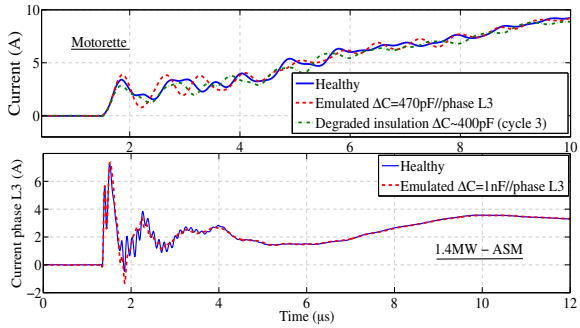

Fig. 13 Transient current response of coil specimen (motorette) and phase L3 of 1.4MW machine.

Again further analysis of the deviation is conducted in the frequency domain by comparing the Fourier components of the amplitude spectrum. In Fig. 14 the spectra of the recorded transient responses of the motorrette at the thermal exposure cycles '*Cycle 0*' to '*Cycle 3*' are depicted. Based on the deviations of the frequency components occurring in the amplitude spectrum between the healthy insulation state and various aged machine winding scenarios, the severity of the insulation deterioration of the motorette is estimated using the insulation state indicator. A tendency of shift resonance peaks to higher frequency values is visible, caused by the reduced capacitance of the specimen after each cycle. This is in accordance to the resonance frequency equation $f_r = 2\pi/\sqrt{LC}$ and increasing frequency at decreasing capacitance. The bar plot represents the calculated indicator values for cycle 0-3. Each cycle is clearly separable and the indicator values show a monotonic increasing tendency.

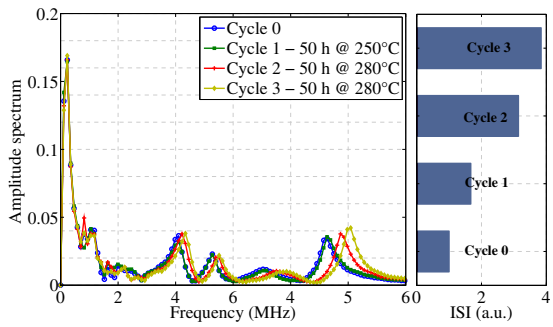

Fig. 14 Spectra of transient current traces and indicators of motorette.

The spectra of the tested scenarios at the 1.4MW induction machine are depicted in Fig. 15. The capacitances are placed parallel to the first coil of phase L3. The winding-to-ground capacitance is estimated with common mode operation and RLC measurement to 21nF per phase. However, the value depends on the considered frequency range and is volatile in the several MHz range.

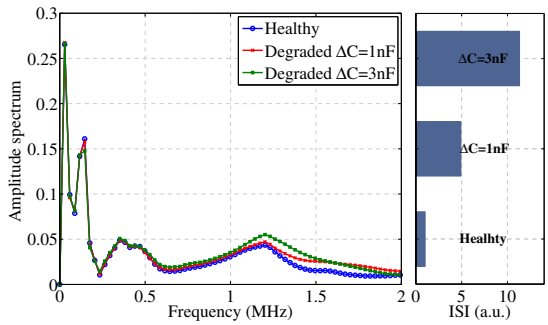

Fig. 15 Spectra of transient current traces and indicators of 1.4MW machine.

The effective winding-to-ground capacitance is the value where the corresponding phase of the impedance is -90°. The capacitances e.g. turn-to-turn capacitance, phase-to-ground capacitance could only be estimated with enhanced models of the ASM or are estimated based on the geometrical dimensions. In the steady-state model of the ASM, cf. [15], no parasitic capacitances are considered. However, the challenge at higher frequencies is that the electrical behavior of the machine changes between being capacitive and inductive. In [16] the model is enhanced by capacitors representing the effective winding-to-frame capacitance as well as the winding to frame capacitance and is an evidence for the estimation of the parameters. Additionally, with the geometrical dimension and dielectric properties, e.g. relative permittivity of the insulation material between the turns, length of the strand respectively the width and the thickness of the insulation, turn-to-turn capacitance is estimated with 1nF. Thus the tested and detected capacitance changes on the 1.4MW machine represent realistic changes scenarios.

V. Conclusion

Inverter-fed machines insulation suffers due to the increasing inverter switching frequencies and very short voltage rise times. At the machine-terminal overvoltages and high frequency oscillations occur and are also visible in the current signal. Based on evaluation of the machine's transient current response and analyzing the frequency components compared to a known healthy insulation state allows for a monitoring of the insulation degradation. Thus down times can be avoided and maintenance on demand scheduled. The applicability of the method was tested on a small 5.5kW random-wound machine and a 1.4MW machine with form-wound stator coils, as well as with IGBT and SiC-MOSFET inverter with different dv/dt-characteristics.

The widespread usage of wide band gap power modules, e.g. SiC-MOSFET, in modern drive systems has not yet taken place. However, since the cost of SiC devices have now started to decrease their application will thus be more common in the next five to ten years. A challenge regarding the high switching frequencies and di/dt will be the radiated and conducted noise influencing the accuracy of the transient current evaluation.

Regarding the economic costs, the high sampling rate additionally demands the usage of higher sampling ADC units or at least enhanced sampling methods, e.g. repetitive sampling.

Acknowledgment

The work was supported by the Austrian Research Promotion Agency (FFG) project number 838478.

References

[1] Oswald, N.; Anthony, P.; McNeill, N.; Stark, B.H., "An Experimental Investigation of the Tradeoff between Switching Losses and EMI Generation With Hard-Switched All-Si, Si-SiC, and All-SiC Device Combinations," *IEEE Trans. on Power Electronics*, vol.29, no.5, pp.2393-2407, May 2014.

[2] IEEE Committee Report, "Report of large motor reliability survey of industrial and commercial installation, Part I," *IEEE Trans. on Industry Applications*, vol.21, pp.853–864, 1985.

[3] IEEE Committee Report, "Report of large motor reliability survey of industrial and commercial installation, Part II," *IEEE Trans. on Industry Applications*, vol.21, pp.865–872, 1985.

[4] Kaufhold, M.; Aninger, H.; Berth, M.; Speck, J.; Eberhardt, M., "Electrical stress and failure mechanism of the winding insulation in PWM-inverter-fed low-voltage induction motors," *IEEE Trans. on Ind. Electronics, vol.47, no.2, pp.396-402,* 2000.

[5] Stone, G. C.; Boulter, E. E.; Culbert, I.; Dhirani, H., "Electrical Insuation for Rotating Machines". *IEEE Press*, 2004.

[6] Neti, P.; Grubic, S., "Online broadband insulation spectroscopy of induction machines using signal injection," *2014 IEEE Energy Conversion Congress and Exposition (ECCE)*, pp.630-637, 2014.

[7] Perisse, F.; Werynski, P.; Roger, D., "A New Method for AC Machine Turn Insulation Diagnostic Based on High Frequency Resonances," *IEEE Trans. on Dielectrics and Electrical Ins.*, vol.14, no.5, 2007.

[8] Grubic, S.; Restrepo, J.; Habetler, T.G., "Online Surge Testing Applied to an Induction Machine With Emulated Insulation Breakdown," *IEEE Trans. on Industry Applications*, vol.49, no.3, pp.1358-1366,2013.

[9] Knockaert, J.; Peuteman, J.; Catrysse, J.; Belmans, R., "Hidden reflection phenomena on inverter-fed induction motors," *European Conference on Power Electronics and Applications*, pp.9 pp.-P.9, 2005.

[10] Amarir, S.; Al-Haddad, K., "Mathematical analysis and experimental validation of transient over-voltage higher than 2 per unit along industrial ASDM long cables," *IEEE Power Electronics Specialists Conference*, pp.1846-1851, 2008.

[11] Von Jouanne, A.; Enjeti, P. N.; "Design considerations for an inverter output filter to mitigate the effects of long motor leads in ASD applications," *IEEE Transactions on Industry Applications*, vol. 33, no. 5, pp. 1138-1145, Sep/Oct 1997.

[12] Skibinski, G.; Tallam, R.; Reese, R.; Buchholz, B.; Lukaszewski, R.; "Common Mode and Differential Mode Analysis of Three Phase Cables for PWM AC Drives," *IEEE Industry Applications Conference Forty-First IAS Annual Meeting*, Tampa, FL, 2006.

[13] Binder, A.; Muetze, A.; "Scaling Effects of Inverter-Induced Bearing Currents in AC Machines," *IEEE Trans. on Industry Applications*, vol. 44, no. 3, pp. 769-776, 2008.

[14] Zoeller, C.; Vogelsberger, M. A.; Fasching, R.; Grubelnik, W.; Wolbank, T. M.; "Evaluation and current-response based identification of insulation degradation for high utilized electrical machines in railway application," *IEEE Diagnostics for Electrical Machines, Power Electronics and Drives (SDEMPED)*, pp. 266-272, 2015.

[15] Mirafzal, B.; Skibinski, G. L.; Tallam, R. M.; Schlegel, D. W.; Lukaszewski, R. A., "Universal Induction Motor Model With Low-to-High Frequency-Response Characteristics," *IEEE Trans. on Industry Applications*, vol. 43, no. 5, pp. 1233-1246, 2007.

[16] Skibinski, G.; Kerkman, R.; Leggate, D.; Pankau, J.; Schlegel, D., "Reflected wave modeling techniques for PWM AC motor drives," *13th Annual Applied Power Electronics Conference and Exposition, APEC*, pp. 1021-1029 vol.2, 1998.